The Astrophysical Journal, 963:149 (8pp), 2024 March 10 https://doi.org/10.3847/1538-4357/ad24ee

Pair Creation in Hot Electrosphere of Compact Astrophysical Objects

Mikalai Prakapenia[1,2] and Gregory Vereshchagin[1,3,4,5]
[1] ICRANet-Minsk, Institute of Physics, National Academy of Sciences of Belarus, 220072 Nezalezhnasci Avenue 68-2, Minsk, Belarus
[2] Department of Theoretical Physics and Astrophysics, Belarusian State University, Nezalezhnasci Avenue 4, 220030 Minsk, Belarus
[3] ICRANet, 65122 Piazza della Repubblica, 10, Pescara, Italy
[4] ICRA, Dipartimento di Fisica, Sapienza Università di Roma, Piazzale Aldo Moro 5, I-00185 Rome, Italy
[5] INAF—Istituto di Astrofisica e Planetologia Spaziali, 00133 Via del Fosso del Cavaliere, 100, Rome, Italy
Received 2023 November 27; revised 2024 January 23; accepted 2024 January 30; published 2024 March 8

Abstract

The mechanism of pair creation in the electrosphere of compact astrophysical objects such as quark stars or neutron stars is revisited, paying attention to evaporation of electrons and acceleration of electrons and positrons, which were previously not addressed in the literature. We perform a series of numerical simulations using the Vlasov–Maxwell equations. The rate of pair creation strongly depends on electric field strength in the electrosphere. Although Pauli blocking is explicitly taken into account, we find no exponential suppression of the pair creation rate at low temperatures. The luminosity in pairs increases with temperature and it may reach up to $L_{\pm} \sim 10^{52}\,\mathrm{erg\,s^{-1}}$, much larger than previously assumed.

Unified Astronomy Thesaurus concepts: Compact objects (288)

1. Introduction

Quantum electrodynamics predicts vacuum breakdown in strong electric field, leading to prolific creation of electron-positron pairs. The extreme value of electric field strength required for this process $E \sim E_c = m_e^2 c^3/\hbar e \simeq 1.3 \times 10^{16}\,\mathrm{V\,cm^{-1}}$, where m_e is the electron mass, e is its charge, c is the speed of light and $\hbar$ is reduced Planck constant, is not yet reachable in laboratory conditions. However, one may look for this process in some extreme astrophysical environments, for reviews see Ruffini et al. (2010) and Vereshchagin & Prakapenia (2022). Indeed, strong electric fields may exist on the bare surfaces of hypothetical quark stars (Alcock et al. 1986; Kettner et al. 1995; Usov 1998; Usov et al. 2005; Harko & Cheng 2006; Picanço Negreiros et al. 2010; Issifu et al. 2023) or even neutron stars (Rotondo et al. 2011a, 2011b; Belvedere et al. 2012; Rueda et al. 2014). The region with overcritical $E > E_c$ electric field in these objects is called the *electrosphere*. Similar electrospheres are predicted for such hypothetical objects as superheavy nuclei (Migdal et al 1976) and quark nuggets (Forbes et al. 2010). The magnitude of the electric field in the electrosphere depends on the sharpness of the boundary of the positively charged component (Mishustin et al. 2010). Usov (1998) in his seminal paper proposed that hot quark stars may be a source of pair winds, potentially observable at cosmological distances. Based on this work, detailed study of particle interactions was performed by Aksenov et al. (2004, 2005) predicting observed properties of hot quark stars.

Recent study of quark stars has focused on their evolution within full general relativity (Zhou et al. 2021; Zhu & Rezzolla 2021), their cooling (Zapata et al. 2022), finite temperature effects (Chu et al. 2019, 2021), strong rotation (Sun & Huang 2022) and differential rotation (Szkudlarek et al. 2019), effects from the presence of magnetic field (Terrero et al. 2021), limits on possible electric charge (Gonçalves & Lazzari 2020; Estevez-Delgado & Estevez-Delgado 2022), and the effects of modified gravity (Deb et al. 2019). Constraints from gravitational waves observations on strange stars were discussed in Mannarelli & Tonelli (2018) and Cao et al. (2022), and the onstraints on the mass–radius relationship in observations of the compact object HESS J1731-347 were established in Oikonomou & Moustakidis (2023), Rather et al. (2023), and Sagun et al. (2023).

In this paper we revisit Usov's mechanism of pair creation in the electrosphere of compact objects. First, we show that the reasoning under Usov's results contains some flaws. Then, we provide new arguments of how pair creation can operate, and derive the rate of pair creation together with pair luminosity for the electrosphere of a compact astrophysical object. The self-consistent simulations for electron-positron pair creation and electric field evolution in the electrosphere are performed. Our results indicate that a hot electrosphere indeed is a source of strong pair wind. This paper is organized as follows. In Section 2, we describe the original Usov's idea. In Section 3, we derive the rate of pair creation in the electrosphere. In Section 4, we present the main equations and corresponding boundary conditions used for simulations. Our numerical results are presented in Section 5. A discussion and conclusions follow in Section 6.

2. Usov's Mechanism

Usov (1998) was the first to point to the possibility of pair creation in electrosphere of compact astrophysical objects. Since the work by Alcock et al. (1986), it is argued that a supercritical electric field may exist near the surface of bare quark star. This is because the sharpness of the quark star surface is determined by the strong interactions, while degenerate electrons are bound to quarks by electromagnetic interactions. Thus, electron spatial distribution extends to larger, still microscopic, distances. The resulting charged layer generates a strong and overcritical electric field. While an overcritical electric field in vacuum should produce electron-positron pairs, this does not happen at small temperatures. The

reason is that all electronic states in this configuration are fully occupied and the Schwinger process is forbidden. To start the pair creation process, empty electronic states have to be present. This is possible when the quark star is just formed its surface temperature is very hot, $k_{\rm B}T_S \sim \varepsilon_{\rm F} \sim 20\,{\rm MeV}$ (Usov 1998), where $\varepsilon_{\rm F}$ is Fermi energy inside the star, T_S is the temperature of the star, and $k_{\rm B}$ is the Boltzmann constant.

The mechanism proposed by Usov (1998) is the following. Given that the rate of pair creation in overcritical electric field is extremely fast, all empty states below the pair creation threshold are instantly occupied by creating electrons and positrons. Then, the slower process of thermalization of electrons determines the appearance of new empty states for electrons. Positrons are ejected by the electric field. Their outflow leads to an outflow of electrons. The number of created electron-positron pairs $N_\pm$ per unit volume ΔV and unit time is estimated as (Usov 1998):

$$\dot{n}_\pm = \frac{\dot{N}_\pm}{S_R \Delta r_E} \simeq \Delta n_e \,/\tau_{ee}, \tag{1}$$

where S_R is the surface area of electrosphere, Δr_E is its thickness, τ_{ee} is the thermalization timescale of electron–electron collisions, and a dot denotes time derivative. The density of electronic empty states below the pair creation threshold Δn_e in the strong degeneracy approximation $k_{\rm B}T_S \ll \varepsilon_{\rm F}$ is

$$\Delta n_e \simeq \frac{3k_{\rm B}T_S}{\varepsilon_{\rm F}} n_e \exp\left(-\frac{2m_e c^2}{k_{\rm B}T_S}\right), \tag{2}$$

the thermalization timescale τ_{ee} is given by

$$\tau_{ee}^{-1} \simeq \frac{3\alpha}{2\pi^{3/2}} \frac{(k_{\rm B}T_S)^2}{\hbar \varepsilon_{\rm F}} J(\zeta), \tag{3}$$

where $\zeta = 2\alpha^{1/2}\pi^{-1/2}\frac{\varepsilon_{\rm F}}{k_{\rm B}T_S}$, α is the fine structure constant and

$$J(\zeta) = \begin{cases} 51(1 - 19.5\zeta^{-1} + 296\zeta^{-2}), & \zeta > 20, \\ 0.23\zeta^{1.8}, & 1 < \zeta < 20, \\ (1/3)\zeta^3 \ln 2/\zeta, & \zeta < 1. \end{cases} \tag{4}$$

The thickness of the electrosphere Δr_E is given by Usov et al. (2005)

$$\Delta r_E = \left(\frac{3\pi}{2\alpha}\right)^{1/2} \frac{m_e c^2}{e\varphi_0} \frac{\hbar}{m_e c}, \tag{5}$$

where φ_0 is electrostatic potential on the surface of the compact object. For the case of fully degenerate electrons, we have $e\varphi_0 = \frac{3}{4}\varepsilon_{\rm F}$. Thus, for $\varepsilon_{\rm F} = 20\,{\rm MeV}$ one finds $\Delta r_E \simeq 3 \times 10^{-11}$ cm.

It is found that the product $\Delta r_E \Delta n_e$ is independent of the temperature. In addition, since the number of created pairs is considerably smaller than the number of electrons in electrosphere, it is assumed that the structure of electrosphere is not modified by the process of pair creation. Therefore, the key assumption adopted by Usov (1998) and Usov et al. (2005) is that the electric field acts as a catalyst for the Schwinger process and it does not affect the particle dynamics.

According to the Usov mechanism, the process of pair creation continues as long as the temperature remains high enough, $k_{\rm B}T_S > 2m_e c^2$, see Equation (2). At lower temperatures, pair creation is exponentially suppressed.

3. Pair Creation Rate in Electrosphere

Assuming that pairs are not produced due to occupied electron states, one can find a static solution for the Vlasov–Maxwell equations. Strictly speaking, this is true only for fully degenerate electrons. One may assume that quasi-static equilibrium is also possible[6] for nonzero temperatures (Kettner et al. 1995). Electrons in equilibrium obey the Fermi–Dirac statistics with their f_e distribution function

$$f_e = \frac{1}{1 + \exp\left[\left(\sqrt{p^2 + m_e^2} - \mu\right)\Big/ T_S\right]}, \tag{6}$$

where μ is their chemical potential.[7] The chemical equilibrium condition for electrons is

$$\mu = e\varphi, \tag{7}$$

implying that electrons are bound by the electrosphere and also that their distribution function does not depend on time $\partial f_e/\partial t = 0$. The number density of electrons for $T_s \ll \mu$ is (Kettner et al. 1995; Usov et al. 2005)

$$n_e = \frac{\mu^3}{3\pi^2} + \frac{\mu T_S^2}{3}. \tag{8}$$

In ultrarelativistic approximation for electrons, the Poisson equation gives (Alcock et al. 1986; Kettner et al. 1995)

$$\frac{d^2\varphi}{dz^2} = -\frac{4\alpha}{3\pi}[e^2\varphi^3 + \pi^2 T_s^2 \varphi - n_q], \tag{9}$$

where $n_q(z < 0) = (\alpha/3\pi^2)(e^2\varphi_q^3 + \pi^2 T_S \varphi_q)$ is the density of a positively charged core and z is spatial coordinate normal to electrosphere. The electric field $E(z)$ is defined from the electrostatic potential $\varphi(z)$ as $E(z) = -\,d\varphi/dz$. The solution of the electrostatic problem is shown in Figure 1 for selected values of temperature. At the surface $z = 0$, the values of electric field E_0 and electrostatic potential φ_0 can be expressed as (Kettner et al. 1995; Usov et al. 2005):

$$E_0 = \sqrt{\frac{2\alpha}{3\pi}} \sqrt{e^4\varphi_0^4 + 2\pi^2 T^2 e^2 \varphi_0^2}, \tag{10}$$

$$e\varphi_0 = \frac{\varepsilon_{\rm F}(2\pi^2 T^2 + 3\varepsilon_{\rm F}^2)}{4(\pi^2 T^2 + \varepsilon_{\rm F}^2)}. \tag{11}$$

It is important to note that this solution is not fully self-consistent. It ignores thermal evaporation of electrons, and the consequent electrosphere *inflation*. The condition of chemical equilibrium (7) is valid at zero temperature. At nonzero temperatures, some electrons have large enough energies to overcome the Coulomb barrier and leave the electrosphere. Therefore, spatial distribution of electrons as well as electric field in hot electrosphere can extend to much larger distances from the surface than in the cold case. This effect is not accounted for by Equation (9) and is not shown in Figure 1. However, our numerical results clearly demonstrate this effect, see below.

The basic assumption made by Usov (1998) is that the role of the electrosphere is just the creation of electron-positron pairs out of the electric field. Their subsequent evolution is determined by collisions, leading to thermalization. In this

[6] We use the term quasi-static, because at nonzero temperature thermal evaporation of electrons modifies the structure of electrosphere, see below.

[7] In this section and below we use the units with $\hbar = c = k_{\rm B} = 1$.

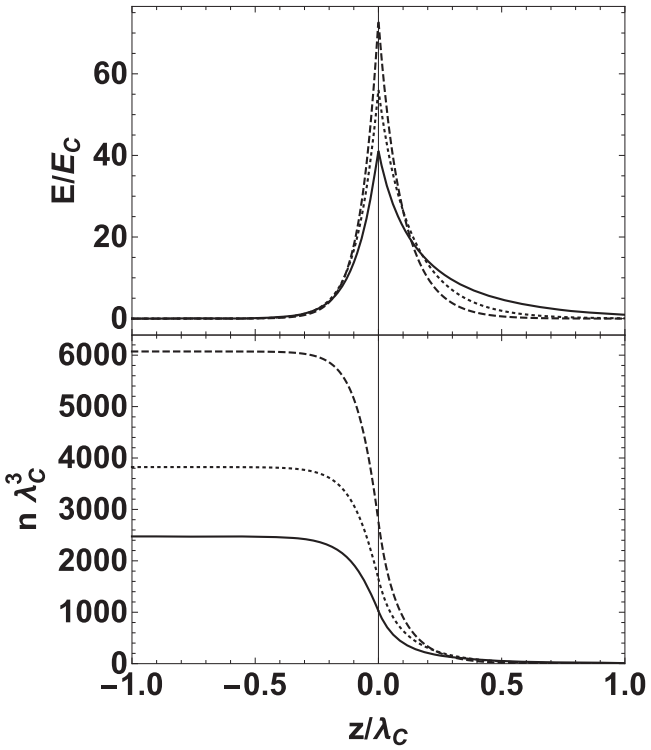

Figure 1. Electric field (top) and electron density (bottom) spatial distribution for selected temperatures T_S: $T_S = 3m_e$ (solid), $T_S = 6m_e$ (dotted), and $T_S = 9m_e$ (dashed). Here, $e\varphi_q = 20$ MeV and $\lambda_C \simeq 2.4 \times 10^{-10}$ cm is electron Compton wavelength.

approach, particle acceleration by the electric field is neglected. While thermalization is indeed relevant process for reaching equilibrium in relativistic plasma (Aksenov et al. 2007, 2009, 2010), there are other kinetic processes that may change electron distribution function. Below we demonstrate that within electrosphere pairs are practically collisionless.

The Coulomb logarithm Λ in relativistic plasma is of the order of unity (Vereshchagin & Aksenov 2017). Hence, the transport cross section for Coulomb collisions of electrons is $\sigma_{\rm coul} = \sigma_{\rm T}(m_e/T_S)^2\Lambda \sim \sigma_{\rm T}$, where $\sigma_{\rm T}$ is the Thomson cross section. Thus, the Thomson cross section can be used as an estimation for the Coulomb scattering cross section. The mean free path l is

$$l \simeq (\sigma_{\rm T} n_e)^{-1} = \frac{3}{8\pi\alpha^2}\left(\frac{n_e}{\lambda_C^{-3}}\right)^{-1}. \tag{12}$$

Assuming that electron density in the electrosphere is $n_e \sim 10^{35}\,{\rm cm}^{-3}$ (Usov 1998), see Figure 1, we obtain $l \sim 10^{-11}$ cm. From these estimations, we see that the thickness of cold electrosphere is equal to the mean free path of particles. As the density of electrons decreases exponentially with radius, it makes the entire region above electrosphere almost collisionless.

We can estimate the rate of pair creation using the Schwinger rate per unit volume and per unit time in a constant in time and homogeneous electric field (Schwinger 1951; Narozhnyi & Nikishov 1970)

$$\dot{n}_\pm = \frac{m_e^4}{4\pi^3}\left(\frac{E}{E_c}\right)^2 \exp\left(-\pi\frac{E_c}{E}\right). \tag{13}$$

To describe pair creation for non-vacuum initial state it is necessary to take into account the Pauli blocking effect (Brodin et al. 2023; Prakapenia & Vereshchagin 2023). We use the differential pair creation rate given by Gatoff et al. (1987) with additional Pauli blocking factor $(1 - f_e)$. The rate is then given by an integral over particle momentum d^3p_e in the following form

$$\dot{n}_\pm = -\frac{2\pi m_e^4}{4\pi^3}\frac{E}{E_c}\int_0^\infty d\tilde{p}\tilde{p}(1-f_e) \times \ln\left[1 - \exp\left(-\frac{\pi(\tilde{p}^2+1)}{E/E_c}\right)\right]. \tag{14}$$

Without the Pauli blocking factor $(1 - f_e)$ this expression reduces to the Schwinger rate (13). Therefore, the rate depends on three parameters: temperature T_S, chemical potential μ, and electric field E. The electric field and chemical potential can be obtained from the electrostatic configuration as a functions of the temperature. The only remaining free parameter is the temperature.

The total rates of pair creation can be computed using the typical parameters for strange stars: $R = 10^6$ cm, $\varepsilon_{\rm F} = 20$ MeV and $\Delta r_E = 10^{-10}$ cm (Alcock et al. 1986; Usov 1998). We show this quantity in Figure 2: the dashed line represents Usov's rate obtained using Equation (1), while the solid line represents the rate computed with Equation (14) and the dotted line corresponds to Equation (15), where the surface quantities (10) were substituted.

At high temperatures $T_S > \varepsilon_{\rm F}$, Pauli blocking becomes negligible and because $E \gg E_c$ one finds (Usov 1998)

$$\dot{N}_\pm \simeq 4\pi R^2 \Delta r_E \frac{m_e^4}{4\pi^3}\left(\frac{E}{E_c}\right)^2 \simeq 4 \times 10^{56}\ {\rm s}^{-1}\left(\frac{E}{5\times 10^{17}{\rm V\,cm}^{-1}}\right)^2. \tag{15}$$

We find that the luminosity in pairs is determined not by their temperature, as Usov assumed, but by the Lorentz factor of the outflow. Positrons are accelerated by the electrosphere and ejected with high Lorentz factor, which can be estimated from the equation of motion

$$\gamma \simeq \frac{E}{E_c}. \tag{16}$$

Electrons, while decelerated in the electrosphere, are dragged together with positrons. In fact, the flux of positrons reduces the Coulomb barrier, thereby allowing more electrons to escape. This guarantees the charge neutrality of the total outflow. From (15) and (16) we find that the luminosity in pairs can be as large as

$$L_\pm \simeq 1.3 \times 10^{52}\ {\rm erg\ s}^{-1}\left(\frac{E}{5\times 10^{17}{\rm V\,cm}^{-1}}\right)^3. \tag{17}$$

In this estimate the reference value of electric field $E = 30E_c$, see Figure 1, in the electrosphere is used. Given the strong dependence on the electric field, even larger values are expected. This result shows that even very large isotropic luminosities of gamma-ray bursts (GRBs) of $10^{53}\,{\rm erg\,s}^{-1}$ and

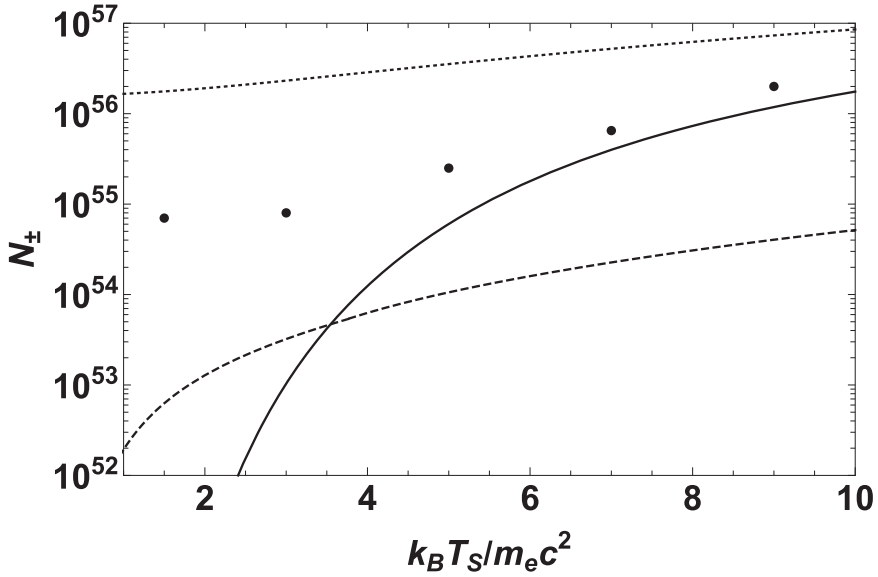

Figure 2. Pair creation rate in the electrosphere $\dot{N}_\pm$ according to Equation (1) for the dashed curve, Equation (15) for the dotted curve and Equation (14) for the solid curve. Dots represent numerical results from the Table 1.

higher are possible for electrosphere of compact objects, provided that $E \sim 80E_c$ or higher at their surface.

The source of energy for pair outflow is the thermal energy of the compact object, which can be as high as 10^{53} erg (Haensel et al. 1991) for the temperatures of 10^{11} K.

Note, that in the derivation of Equation (14), the role of Pauli blocking is overestimated. Pair acceleration by the electric field is so strong that it operates as an alternative mechanism to thermalization by creating empty states in the phase space, and thus allowing pair creation to operate. In order for this mechanism to work, the rate of pair creation obtained from (13) should be smaller than the rate of acceleration, obtained from (16), which leads to the following constraint (Benedetti et al. 2011)

$$\frac{1}{4\pi^3}\frac{E}{E_c}\exp\left(-\pi\frac{E_c}{E}\right) \leqslant 1, \tag{18}$$

which gives $E \lesssim 127E_c$. Therefore, for typical values of electric field in electrosphere, this effect strongly enhances pair creation.

4. Dynamical Equations and Initial Conditions at the Surface

Since we consider particle dynamics in orthogonal direction to the surface of the compact object, we introduce cylindrical coordinates in momentum space $p = \{p_\perp, p_\phi, p_{||}\}$ with $p_{||}$-axis parallel to electric field E. Particle energy is then $p^0 = [p_\perp^2 + p_{||}^2 + m_e^2]^{1/2}$.

Particle evolution is described by one-particle electron/positron distribution function $f_\pm(t, z, p_\perp, p_{||})$, which is normalized on particle density $n_\pm = \int \frac{2d^3p}{(2\pi)^3} f_\pm$.

We introduce dimensionless quantities $\tilde{t} = tm$, $\tilde{z} = zm$, $\tilde{p} = p/m$, $\tilde{E} = Ee/m_e^2$ to write the basic dynamic equations in dimensionless form. The set of Maxwell–Vlasov equations in our case reduces to the Vlasov–Ampére system, which has to be supplemented with the Gauss law, as an initial condition. For this purpose, we use the Poisson Equation (9). We have

$$\begin{aligned}
&\frac{\partial f_\pm}{\partial \tilde{t}} + \frac{\tilde{p}_{||}}{\tilde{p}^0}\frac{\partial f_\pm}{\partial \tilde{z}} \mp \tilde{E}\frac{\partial f_\pm}{\partial \tilde{p}_{||}} \\
&= -(1 - f_+ - f_-)|\tilde{E}| \ln\left[1 - \exp\left(-\frac{\pi(1+\tilde{p}_\perp^2)}{|E|}\right)\right]\delta(\tilde{p}_{||}), \\
&\frac{\partial E}{\partial t} = 8\pi\alpha\int\frac{d^3\tilde{p}}{(2\pi)^3}\frac{\tilde{p}}{\tilde{p}^0}(f_- - f_+) + 16\pi\alpha\frac{|\tilde{E}|}{\tilde{E}}\int\frac{d^3\tilde{p}}{(2\pi)^3}\tilde{p}_0 \\
&\times (1 - f_+ - f_-)\ln\left[1 - \exp\left(-\frac{\pi(1+\tilde{p}_\perp^2)}{|\tilde{E}|}\right)\right]\delta(\tilde{p}_{||}).
\end{aligned} \tag{19}$$

We recall that the static solution of the Vlasov–Ampére system (19) may be obtained from the solution of the Poisson Equation (9) only in the case $T_S = 0$, i.e., for fully degenerate electrons. Only in this case does the chemical potential (7) equal the Fermi energy. This implies that that there are no electrons with energies exceeding the Coulomb barrier. However, when the surface temperature is nonzero $T_S > 0$ there is a small part of electrons with energies larger than the Coulomb barrier. These electrons move outward the surface, increasing the electric field outside the surface of the compact object, andleading to electrosphere inflation.

The initial distribution function of electrons is assumed to be the Fermi–Dirac one (6), where the chemical potential $\mu = e\varphi$ and the temperature T_S are obtained from the Poisson Equation (9). The initial distribution function of electrons at the surface $z = 0$ is shown in Figure 3 for two different values of temperature. The smaller is the temperature, the larger is the degeneracy of electrons at small momenta, where pair creation operates, and one can expect much fewer pairs in this case, see Figure 2.

5. Numerical Results

We integrate numerically the system of Equations (19) and present the results for $T_S = 3m_e$ in Figure 4, and for $T_S = 7m_e$ in Figure 5.

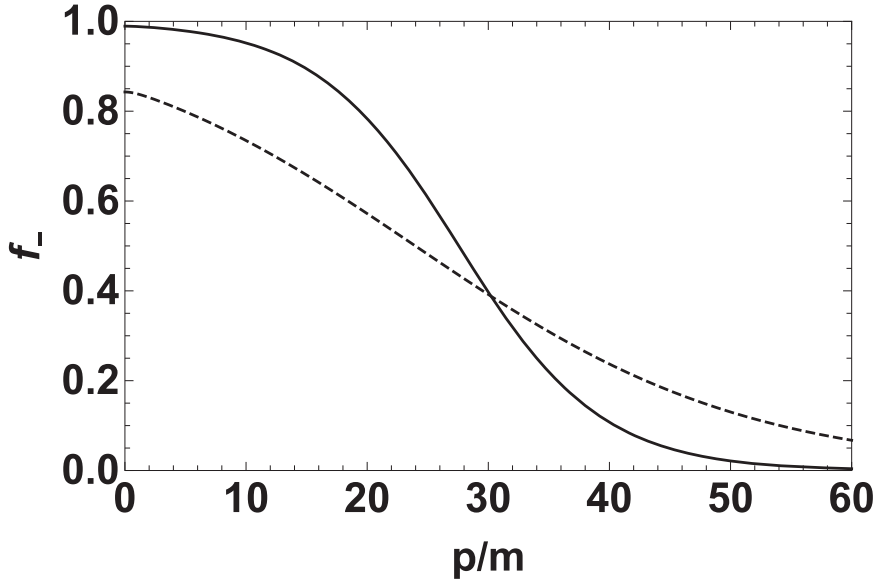

Figure 3. Initial distribution of electrons in the momentum space at the surface $z = 0$ of the compact object for different surface temperatures: $T_S = 3m_e$ (solid) and $T_S = 7m_e$ (dashed).

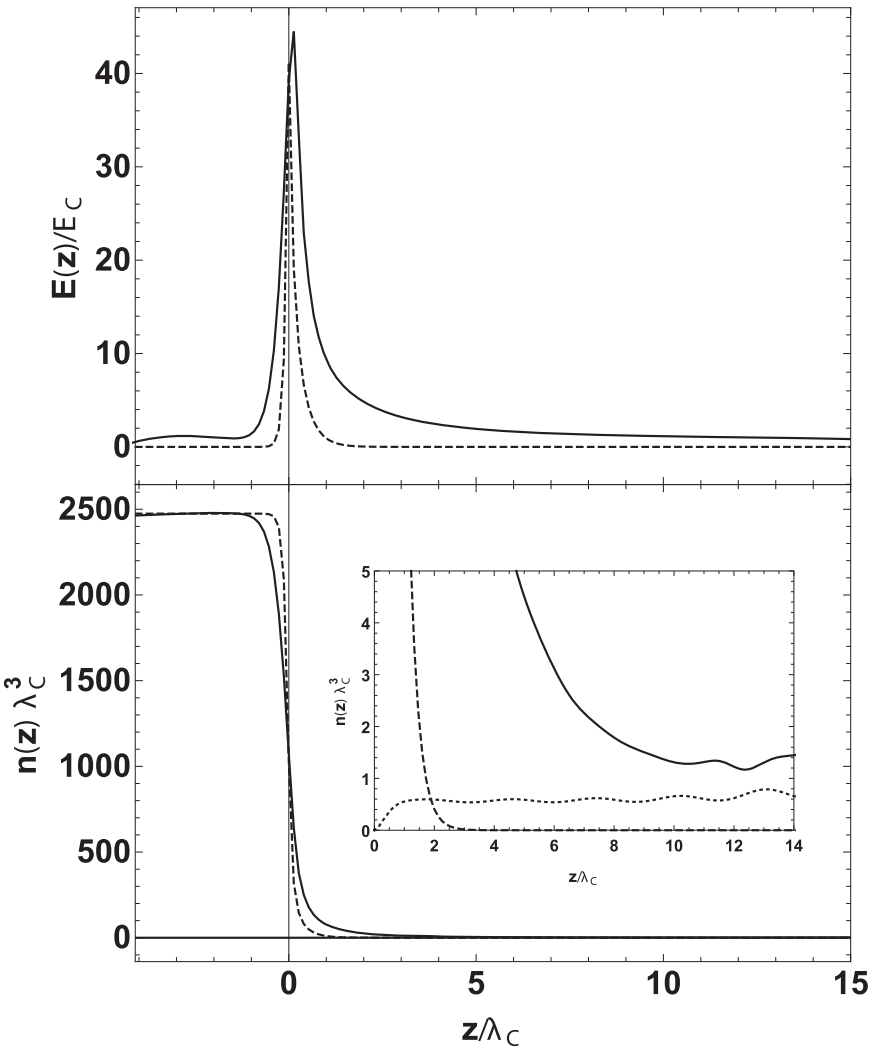

Figure 4. Electric field (top) and electron number density (bottom) as a function of distance from the surface of the compact object. Dashed curves represent electrostatic solution. Solid curves represents inflated electrosphere. The inset shows electron (solid) and positron (dotted) spatial distribution. Here $T_S = 3m_e$.

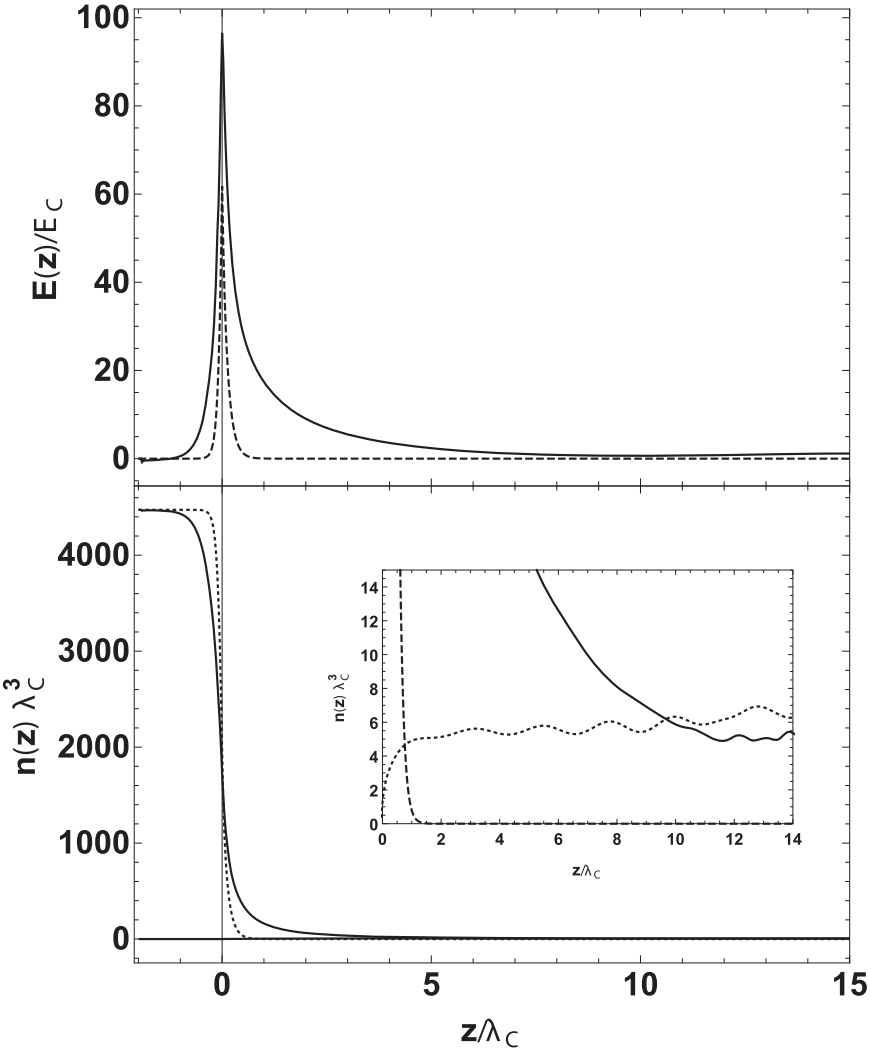

Figure 5. The same as in Figure 4 for $T_S = 7m_e$.

The electric field and electron number density as function of distance from the surface of the compact object are shown in Figures 4 and 5. The electrostatic solutions of Equation (9), used as initial conditions for simulations, are represented by dashed curves. The solutions of dynamical Equations (19) are shown by solid curves. Electrosphere inflation due to evaporation of electrons, whose energy exceeds the Coulomb barrier, leads to extension of the region of overcritical electric field from $z \sim \lambda_C$ up to $z \sim 10\lambda_C$. Inflation of the electrosphere results in an increase of electrostatic energy by a factor 3 for $T_S = 3m_e$ and by a factor of 7 for $T_S = 7m_e$. This means that much larger energy is available for the acceleration of positrons, compared to the electrostatic case. Electron-positron pairs are mostly produced near the surface at $z = 0$, where the electric field is the largest. The combined flux of electrons and positrons is clearly visible in the insets in Figures 4 and 5 at $z > 10\lambda_C$.

The average energy of electrons and positrons is computed as

$$\langle \tilde{\varepsilon}_{\pm} \rangle = \frac{1}{\tilde{n}_{\pm}} \int 2 \frac{d^3\tilde{p}}{(2\pi)^3} \tilde{p}^0 f_{\pm}. \tag{20}$$

In Figure 6, we present this quantity as a function of distance from the surface. It is clear that the Coulomb barrier located as small z decelerates electrons and accelerates positrons. At larger distances, positrons are additionally accelerated by the inflated electrosphere. The Lorentz factor γ of the outflow here is approximately equal to the average energy. Specifically, we find $\gamma \simeq 40$ for $T_S = 3m_e$ and $\gamma \simeq 50$ for $T_S = 7m_e$, in agreement with the estimate (16).

Finally, we compute the luminosity of the outflow at a distance $\tilde{z}$ from the boundary as follows

$$\tilde{L} = 4\pi(\tilde{R} + \tilde{z})^2 \int 2 \frac{d^3\tilde{p}}{(2\pi)^3} \tilde{p}_{||}(f_+ + f_-). \tag{21}$$

The peak luminosity for $R = 10$ km and $T_S = 3m_e$ is $L \simeq 2 \times 10^{50}$ erg s^{-1}. For $T_S = 7m_e$, we obtain $L \simeq 4 \times 10^{51}$ erg s^{-1}. The values $\dot{N} \simeq L/\langle \tilde{\varepsilon}_{\pm} \rangle$ are 6×10^{54} s^{-1} and 10^{56} s^{-1}, respectively, see Figure 2.

Note that the average density of pairs for $T_S = 3m_e$ is about one pair in Compton volume, namely $n_{\pm} \simeq 7 \times 10^{28}$ cm^{-3}. For $T_S = 7m_e$ we find $n_{\pm} \simeq 4 \times 10^{29}$ cm^{-3}. These densities are much smaller than the density of electrons at the boundary $z = 0$. The mean free path (12) is $2 \times 10^3 \lambda_C$ and $1.2 \times 10^4 \lambda_C$ respectively, which is much larger than the Compton length. On such distances from the boundary, the outflow is collisionless and does not thermalize. We also performed

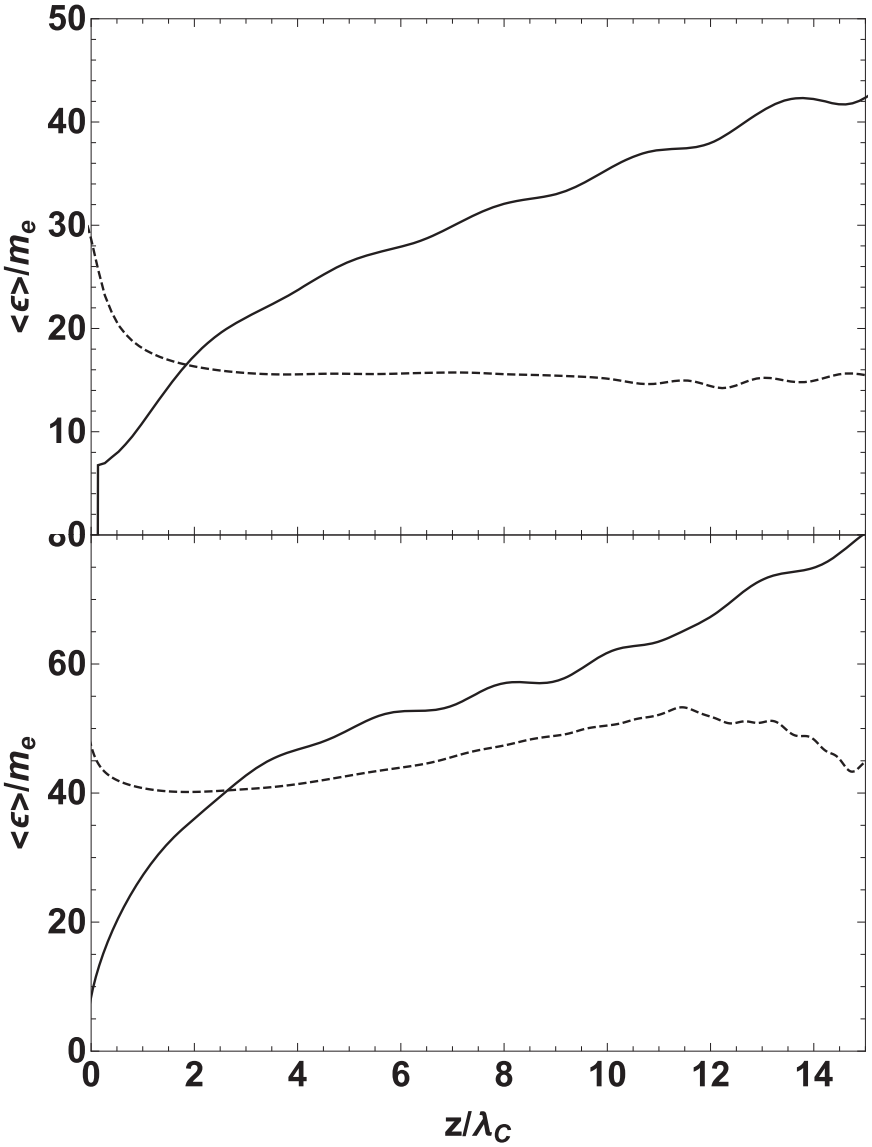

Figure 6. Average energy of electrons (dashed) and positrons (solid) for $T_S = 3m_e$ (top) and $T_S = 7m_e$ (bottom) as a function of distance from the surface.

Table 1
Average Pair Creation Rate Given by Usov Equation (1) $\dot{N}_{\pm}^{U}$, $\dot{N}_{\pm}$, Average Luminosity $L_{\pm}$, Average Energy per Particle of Electrons $\langle\tilde{\varepsilon}_{-}\rangle$ and Positrons $\langle\tilde{\varepsilon}_{+}\rangle$ Obtained from Numerical Simulations at $t = 17\lambda_C/c$ for Selected Temperatures T_S

T_S	$1.5m_e$	$3m_e$	$5m_e$	$7m_e$	$9m_e$
$\dot{N}_{\pm}^{U}$, s^{-1}	6×10^{52}	3×10^{53}	1×10^{54}	2×10^{54}	4×10^{54}
$\dot{N}_{\pm}$, s^{-1}	7×10^{54}	8×10^{54}	3×10^{55}	6×10^{55}	2×10^{56}
$L_{\pm}$, erg s^{-1}	1×10^{50}	2×10^{50}	1×10^{51}	4×10^{51}	1×10^{52}
$\langle\tilde{\varepsilon}_{-}\rangle$	8	16	27	46	68
$\langle\tilde{\varepsilon}_{+}\rangle$	12	30	45	54	65

simulations for $T_S = 1.5m_e$, $T_S = 5m_e$ and $T_S = 9m_e$. All of the results are collected in Table 1. The numerical rate of pair creation is also represented in Figure 2. We note that Usov's rate of pair creation is underestimated by about two orders of magnitude. It is clear that the values of pair creation rate and luminosity exceed the estimates based on Usov's formula (1) and the estimates, which assume steady Pauli blocking (14). However, these values are smaller than the maximum rate (15) computed in the absence of Pauli blocking.

6. Discussion and Conclusions

Our kinetic simulation reveals two physical effects in the hot electrosphere, which were ignored in previous analyses. The first effect is the inflation of the electrosphere due thermal evaporation of electrons, leading to its spatial extension to distances much larger than the electrostatic solution implies. In addition, increased electrostatic energy implies stronger acceleration of the positrons and a corresponding increase in the luminosity of the outflow. The second effect is the enhancement of the rate of pair creation due to pair simultaneous acceleration by the electric field. Both effects are crucial for the estimation of the pair creation rate, especially at low temperatures with strongly degenerate electrons, where analytical formulas fail to reproduce numerical rates, see Figure 2.

Our numerical results show that, as expected, the Schwinger process operates for nonzero temperature T_S. Positrons are accelerated in the Coulomb barrier and move outward. The total outward flux is approximately neutral due ability of electrons to overcome the Coulomb barrier. The distribution of the electric field and electron density is quasi-static and pair creation does not back react on the electrosphere. As a result, electrons do not occupy all empty states and the process operates continuously.

In our simulations, the interior of the compact object serves as a thermal bath of electrons. In the absence of collisions, electrons with negative momentum are absorbed in the interior and equal number of electrons with positive momentum are created. Such mirror boundary conditions are adopted to ensure the energy and particle conservation on the finite computational grid. We do not investigate in this paper the fate of electrons moving inward because we consider collisionless dynamics. It is expected that Coulomb collisions thermalize these electrons.

We also do not discuss the thermal evolution of the compact object and its impact on pair luminosity. It is expected that on a sufficiently long timescale, the temperature should decrease sufficiently to halt the Schwinger process. It has been argued by Page & Usov (2002) that neutrino cooling leads to rapid decrease of the surface temperature below MeV values. However, it was recently shown by Li et al. (2021) that quark stars at high temperatures are opaque to neutrinos. Since neutrinos are captured within neutrinosphere, the cooling is less efficient.

Clearly, on larger distances from the electrosphere pair the outflow becomes collisional. Interaction between electrons and positrons eventually produces photons. Kinetic simulations of this process has been reported by Aksenov et al. (2004, 2005) assuming that their rate is given by Usov's formula (1).

Our conclusion is that hot compact objects with an overcritical electric field on their surface may produce much stronger electron-positron pair outflows than previously thought. Given that their luminosity may reach up to $10^{53}\,\mathrm{erg\,s^{-1}}$, they may be relevant for emission from gamma-ray bursts and soft gamma repeaters.

To summarize, in this paper we revisit Usov's mechanism for pair creation in the electrospheres of compact astrophysical objects, such as hypothetical quark stars or neutron stars. As the density of electrons rapidly decreases outside the surface, electrosphere is essentially collisionless and pair dynamics is governed by the Vlasov–Maxwell equations. By numerically solving these equations for the hot electrosphere, we found two effects, which were previously ignored in the literature. First, due to thermal evaporation of electrons, the electrosphere is inflated to much larger distances, though still microscopic, than electrostatic solution implies. Second, even for a strongly degenerate distribution of electrons in the electrosphere, Pauli blocking is efficiently reduced by simultaneous acceleration of pairs created by the Schwinger process. Both of these effects dramatically enhance pair creation rate, leading to luminosities that can be as large as $10^{52}\,\mathrm{erg\,s^{-1}}$, see Equation (15), much larger than previously derived.

These results imply that a hot electrosphere may be a stronger source of relativistic pair outflows than previously assumed. Electron-positron pairs are generated in the electrosphere in a collisionless regime.

Acknowledgments

We thank the anonymous referee for the comments, which allowed us to improve the presentation of our results. This work is supported within the joint BRFFR-ICRANet-2023 funding program under grant No. F23ICR-001.

References

Aksenov, A. G., Milgrom, M., & Usov, V. V. 2004, ApJ, 609, 363
Aksenov, A. G., Milgrom, M., & Usov, V. V. 2005, ApJ, 632, 567
Aksenov, A. G., Ruffini, R., & Vereshchagin, G. V. 2007, PhRvL, 99, 125003
Aksenov, A. G., Ruffini, R., & Vereshchagin, G. V. 2009, PhRvD, 79, 043008
Aksenov, A. G., Ruffini, R., & Vereshchagin, G. V. 2010, PhRvE, 81, 046401
Alcock, C., Farhi, E., & Olinto, A. 1986, ApJ, 310, 261
Belvedere, R., Pugliese, D., Rueda, J. A., Ruffini, R., & Xue, S.-S. 2012, NuPhA, 883, 1
Benedetti, A., Han, W.-B., Ruffini, R., & Vereshchagin, G. V. 2011, PhLB, 698, 75
Brodin, G., Al-Naseri, H., Zamanian, J., Torgrimsson, G., & Eliasson, B. 2023, PhRvE, 107, 035204
Cao, Z., Chen, L.-W., Chu, P.-C., & Zhou, Y. 2022, PhRvD, 106, 083007
Chu, P.-C., Jiang, Y.-Y., Liu, H., et al. 2021, EPJC, 81, 569
Chu, P.-C., Zhou, Y., Li, X.-H., & Zhang, Z. 2019, PhRvD, 100, 103012
Deb, D., Ketov, S. V., Khlopov, M., & Ray, S. 2019, JCAP, 2019, 070
Estevez-Delgado, J., & Estevez-Delgado, G. 2022, CQGra, 39, 085005
Forbes, M. M., Lawson, K., & Zhitnitsky, A. R. 2010, PhRvD, 82, 083510
Gatoff, G., Kerman, A. K., & Matsui, T. 1987, PhRvD, 36, 114
Gonçalves, V. P., & Lazzari, L. 2020, PhRvD, 102, 034031
Haensel, P., Paczynski, B., & Amsterdamski, P. 1991, ApJ, 375, 209
Harko, T., & Cheng, K. S. 2006, ApJ, 643, 318
Issifu, A., da Silva, F. M., & Menezes, D. P. 2023, arXiv:2311.12511
Kettner, C., Weber, F., Weigel, M. K., & Glendenning, N. K. 1995, PhRvD, 51, 1440
Li, S.-Z., Yu, Y.-W., Gao, H., Dai, Z.-G., & Zheng, X.-P. 2021, ApJ, 922, 214
Mannarelli, M., & Tonelli, F. 2018, PhRvD, 97, 123010
Migdal, A. B., Voskresenskiĭ, D. N., & Popov, V. S. 1976, JETPL, 24, 163
Mishustin, I. N., Ebel, C., & Greiner, W. 2010, JPhG, 37, 075201
Narozhnyi, N., & Nikishov, A. 1970, SvJNP, 11, 596
Oikonomou, P. T., & Moustakidis, C. C. 2023, PhRvD, 108, 063010
Page, D., & Usov, V. V. 2002, PhRvL, 89, 131101
Picanço Negreiros, R., Mishustin, I. N., Schramm, S., & Weber, F. 2010, PhRvD, 82, 103010
Prakapenia, M., & Vereshchagin, G. 2023, PhRvD, 108, 013002
Rather, I. A., Panotopoulos, G., & Lopes, I. 2023, EPJC, 83, 1065
Rotondo, M., Rueda, J. A., Ruffini, R., & Xue, S. S. 2011a, PhLB, 701, 667
Rotondo, M., Rueda, J. A., Ruffini, R., & Xue, S. S. 2011b, PhRvC, 83, 045805
Rueda, J. A., Ruffini, R., Wu, Y.-B., & Xue, S.-S. 2014, PhRvC, 89, 035804
Ruffini, R., Vereshchagin, G., & Xue, S.-S. 2010, PhR, 487, 1
Sagun, V., Giangrandi, E., Dietrich, T., et al. 2023, ApJ, 958, 49
Schwinger, J. 1951, PhRv, 82, 664
Sun, F., & Huang, A. 2022, PhRvD, 106, 076007
Szkudlarek, M., Gondek-Rosińska, D., Villain, L., & Ansorg, M. 2019, ApJ, 879, 44
Terrero, D. A., Pérez, S. L., Paret, D. M., Martínez, A. P., & Angulo, G. Q. 2021, PhRvC, 103, 045807
Usov, V. V. 1998, PhRvL, 80, 230
Usov, V. V., Harko, T., & Cheng, K. S. 2005, ApJ, 620, 915
Vereshchagin, G., & Prakapenia, M. 2022, Univ, 8, 473
Vereshchagin, G. V., & Aksenov, A. G. 2017, Relativistic Kinetic Theory (Cambridge: Cambridge Univ. Press)
Zapata, J., Sales, T., Jaikumar, P., & Negreiros, R. 2022, A&A, 663, A19
Zhou, E., Kiuchi, K., Shibata, M., Tsokaros, A., & UryÅ, K. 2021, PhRvD, 103, 123011
Zhu, Z., & Rezzolla, L. 2021, PhRvD, 104, 083004